



# Institute of Theoretical and Experimental Physics

15-00

R. Arnold, C. Augier, J. Baker, A. Barabash,  
D. Blum, V. Brudanin, A.J. Caffrey, J.E. Campagne,  
E. Caurier, D. Dassié, V. Egorov, T. Filipova,  
R. Gurriaran, J.L. Guyonnet, F. Hubert, Ph. Hubert,  
S. Jullian, I. Kisel, O. Kochetov, V.N. Kornoukhov,  
V. Kovalenko, D. Lalanne, F. Laplanche, F. Leccia,  
I. Linck, C. Longuemare, Ch. Marquet, F. Mauger,  
H.W. Nicholson, I. Pilugin, F. Piquemal, J-L. Reyss,  
X. Sarazin, F. Scheibling, J. Suhonen, C.S. Sutton,  
G. Szklarz, V. Timkin, R. Torres, V. Umatov,  
I. Vanyushin, A. Vareille, V. Vasilyev, Ts. Vylov

Limits on different Majoron decay  
modes of  $^{100}\text{Mo}$ ,  $^{116}\text{Cd}$ ,  $^{82}\text{Se}$  and  $^{96}\text{Zr}$   
for neutrinoless double beta decays in  
the NEMO-2 experiment.

CERN LIBRARIES, GENEVA



SCAN-0009278

M o s c o w      2000

0.19548

LIMITS ON DIFFERENT MAJORON DECAY MODES OF  $^{100}\text{Mo}$ ,  $^{116}\text{Cd}$ ,  $^{82}\text{Se}$  AND  $^{96}\text{Zr}$   
FOR NEUTRINOLESS DOUBLE BETA DECAYS IN THE NEMO-2 EXPERIMENT:  
Preprint ITEP 15-00/

R. Arnold<sup>11</sup>, C. Augier<sup>9</sup>, J. Baker<sup>5</sup>, A. Barabash<sup>8</sup>, D. Blum<sup>9</sup>, V. Brudanin<sup>3</sup>, A.J. Caffrey<sup>5</sup>, J.E. Campagne<sup>9</sup>, E. Caurier<sup>11</sup>, D. Dassié<sup>1</sup>, V. Egorov<sup>3</sup>, T. Filipova<sup>3,9</sup>, R. Gurriaran<sup>1</sup>, J.L. Guyonnet<sup>11</sup>, F. Hubert<sup>1</sup>, Ph. Hubert<sup>1</sup>, S. Jullian<sup>9</sup>, I. Kisel<sup>3</sup>, O. Kochetov<sup>3</sup>, V.N. Kornoukhov<sup>8</sup>, V. Kovalenko<sup>3</sup>, D. Lalanne<sup>9</sup>, F. Laplanche<sup>9</sup>, F. Leccia<sup>1</sup>, I. Linck<sup>11</sup>, C. Longuemare<sup>2</sup>, Ch. Marquet<sup>1</sup>, F. Mauger<sup>2</sup>, H.W. Nicholson<sup>10</sup>, I. Pilugin<sup>8</sup>, F. Piquemal<sup>1</sup>, J-L. Reyss<sup>4</sup>, X. Sarazin<sup>9</sup>, F. Schibling<sup>11</sup>, J. Suhonen<sup>6</sup>, C.S. Sutton<sup>10</sup>, G. Szklarz<sup>9</sup>, V. Timkin<sup>3</sup>, R. Torres<sup>1</sup>, V. Umatov<sup>8</sup>, I. Vanyushin<sup>8</sup>, A. Vaille<sup>1</sup>, V. Vasilyev<sup>8</sup>, Ts. Vylov<sup>3</sup> - M., 2000 - 16p.

The NEMO-2 tracking detector located in the Fréjus Underground Laboratory was designed as a prototype for the NEMO-3 detector and to study different modes of double beta decay. Measurements with  $^{100}\text{Mo}$ ,  $^{116}\text{Cd}$ ,  $^{82}\text{Se}$  and  $^{96}\text{Zr}$  were carried out. Presented here are the experimental half-life limits on double beta decays for new Majoron emission modes and limits on effective neutrino-Majoron coupling constants.

ОГРАНИЧЕНИЯ НА РАСПАДЫ С ИСПУСКАНИЕМ МАЙОРОНА  $^{100}\text{Mo}$ ,  $^{116}\text{Cd}$ ,  $^{82}\text{Se}$  И  $^{96}\text{Zr}$  ИЗ ЭКСПЕРИМЕНТА NEMO-2.

Детектор NEMO-2, расположенный в подземной лаборатории Фреджус, был разработан как прототип детектора NEMO-3 для изучения различных каналов двойного бета-распада. Были проведены измерения с изотопами  $^{100}\text{Mo}$ ,  $^{116}\text{Cd}$ ,  $^{82}\text{Se}$  и  $^{96}\text{Zr}$ . В работе представлены экспериментальные пределы на новые модели двойного бета-распада с испусканием Майорона, а также пределы на эффективную константу связи Майорона и нейтрино.

Fig. - 3, ref. - 41 names.

© Институт теоретической и экспериментальной физики, 1999

<sup>1</sup>CENBG, IN2P3-CNRS et Université de Bordeaux, 33170 Gradignan, France

<sup>2</sup>LPC, IN2P3-CNRS et Université de Caen, 14032 Caen, France

<sup>3</sup>JINR, 141980 Dubna, Russia

<sup>4</sup>CFR, CNRS, 91190 Gif sur Yvette, France

<sup>5</sup>INEEL, Idaho Falls, ID 83415, U.S.A.

<sup>6</sup>JYVÄSKYLÄ University, 40351 Jyväskylä, Finland

<sup>7</sup>INR, 252028 Kiev, Ukraine

<sup>8</sup>ITEP, 117259 Moscow, Russia

<sup>9</sup>LAL, IN2P3-CNRS et Université Paris-Sud, 91405 Orsay, France

<sup>10</sup>MHC, South Hadley, Massachusetts 01075, U.S.A.

<sup>11</sup>IReS, IN2P3-CNRS et Université Louis Pasteur, 67037 Strasbourg, France.

## 1. Introduction

Spontaneous violation of global (B-L) symmetry in gauge theories leads to the existence of a massless Goldstone boson, the Majoron. At the beginning of the 1980's there were considered to be singlet [1], doublet [2] and triplet [3] Majoron models. All these models resulted in the neutrinoless double beta ( $2\beta$ ) decay with the emission of a Majoron ( $\chi^0$ ):

$$(A, Z) \rightarrow (A, Z + 2) + 2e^- + \chi^0 \quad (1)$$

However, the interaction of the triplet (or doublet) Majorons with the  $Z^0$  boson would give a contribution to the width of the  $Z^0$  decay, which corresponds to two (or 1/2) additional massless neutrino types (see for example [4, 5, 6]). LEP data gives  $2.994 \pm 0.012$  neutrino types [7], thus triplet and some doublet Majorons are excluded. Nevertheless, in reference [8] it is proposed, that a small gauge coupling constant does not eliminate the possibility of a large Yukawa coupling with neutrinos. Thus, the singlet and doublet Majorons can still contribute to neutrinoless  $2\beta$ -decay [8, 9].

Another possibility for neutrinoless  $2\beta$ -decay with Majoron emission arises in supersymmetry models with R-parity violation [9, 10]. It was first stated in [10] that there is the possibility of a  $2\beta\chi^0\chi^0$ -decay with the emission of two Majorons :

$$(A, Z) \rightarrow (A, Z + 2) + 2e^- + 2\chi^0 \quad (2)$$

In the 1990's several new "Majoron" models were suggested. The term "Majoron" here denotes massless or light bosons with a coupling to neutrinos.

Table 1. Different Majoron models according to [12, 14]. The mode IIF corresponds to the model of C.D. Carone [13]

Case	Decay mode	Goldstone boson	L	n	Matrix element
IB	$2\beta\chi^0$	no	0	1	$M_F - M_{GT}$
IC	$2\beta\chi^0$	yes	0	1	$M_F - M_{GT}$
ID	$2\beta\chi^0\chi^0$	no	0	3	$M_{F\omega^2} - M_{GT\omega^2}$
IE	$2\beta\chi^0\chi^0$	yes	0	3	$M_{F\omega^2} - M_{GT\omega^2}$
IIB	$2\beta\chi^0$	no	-2	1	$M_F - M_{GT}$
IIC	$2\beta\chi^0$	yes	-2	3	$M_{CR}$
IID	$2\beta\chi^0\chi^0$	no	-1	3	$M_{F\omega^2} - M_{GT\omega^2}$
IIE	$2\beta\chi^0\chi^0$	yes	-1	7	$M_{F\omega^2} - M_{GT\omega^2}$
IIF	$2\beta\chi^0$	gauge boson	-2	3	$M_{CR}$

In these models "Majoron" can carry a lepton charge, but cannot be a Goldstone boson [11]. Additionally there can be decays with the emission of two "Majorons" [12]. In the models with a vector "Majoron" it is a longitudinal component of the massive gauge boson emitted in  $2\beta$ -decay [13]. All these new objects are called Majorons for simplicity.

In Table 1 there are nine Majoron models presented (following [12, 13, 14]), which are considered in this work. It is divided into two sections, one for lepton number violation and one for lepton number conserving models. The table also shows whether the corresponding  $2\beta$ -decay is accompanied by the emission of one or two Majorons. The next three entries list the main features of the models: the third column lists whether the Majoron is a Goldstone boson or not (or a gauge boson in the case of vector Majorons, type IIF). In column four the leptonic charge  $L$  is given. Column five gives the "spectral index"  $n$  of the summed energy of the emitted electrons, which is defined by the phase space of the emitted particles,  $G \sim (Q_{\beta\beta} - T)^n$ . Here  $Q_{\beta\beta}$  is the energy released in the decay and  $T$  the energy of the two electrons. Energy spectra of different modes of  $2\beta 2\nu$  ( $n = 5$ ),  $2\beta\chi^0$  ( $n = 1$  and  $3$ ) and  $2\beta\chi^0\chi^0$  ( $n = 3$  and  $7$ ) decays are presented in Fig. 1. The different shapes can be used to distinguish the different Majoron decay modes from each other and  $2\beta$ -decay with the emission of two neutrinos. In the last column of Table 1 the nuclear matrix elements (NME) are listed.

Attempts to observe  $2\beta$ -decay with Majoron emission have been undertaken for the last 20 years. Consequently there now exist strong limits on the "standard" Majoron with the "standard" electron energy spectrum shape ( $n = 1$ ),

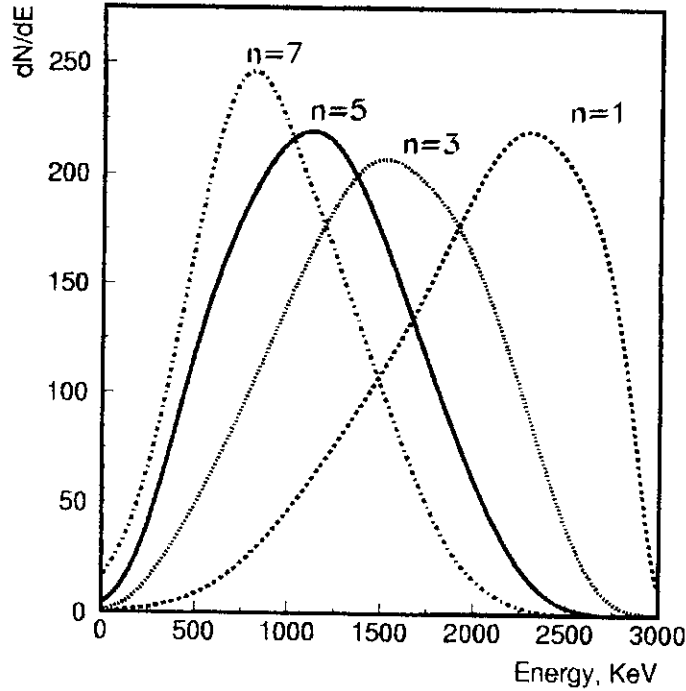


Figure 1. Energy spectra of different modes of  $2\beta 2\nu$  ( $n = 5$ ),  $2\beta\chi^0$  ( $n = 1$  and  $3$ ) and  $2\beta\chi^0\chi^0$  ( $n = 3$  and  $7$ ) decays of  $^{100}\text{Mo}$ .

see Table 2. The best limits on the Majoron coupling constant ( $\langle g_{ee} \rangle$ ) were obtained in experiments with  $^{128}\text{Te}$  [15],  $^{116}\text{Cd}$  [16],  $^{100}\text{Mo}$  [17] and  $^{136}\text{Xe}$  [27] yielding a limit on  $\langle g_{ee} \rangle$  on the level  $\sim 10^{-4}$ . Sufficiently less information exists for "non-standard" Majoron models. The most carefully studied "non-standard" models are being investigated with  $^{76}\text{Ge}$  [18]. There are also limits on decays with the emission of two Majorons in  $^{100}\text{Mo}$  [19] and  $^{116}\text{Cd}$  [20].

In this work a systematic search for  $2\beta$ -decays with different Majoron types was carried out for  $^{100}\text{Mo}$ ,  $^{116}\text{Cd}$ ,  $^{82}\text{Se}$  and  $^{96}\text{Zr}$ , using the experimental data obtained with the NEMO-2 detector [21]. Limits on the standard Majoron ( $n = 1$ ) were published earlier [16, 22, 23, 24].

## 2. NEMO-2 detector

The NEMO-2 detector (Fig. 2) consists of a  $1\text{m}^3$  tracking volume filled with helium gas and 4% ethyl alcohol. Vertically bisecting the detector is the plane of the source foil ( $1\text{m} \times 1\text{m}$ ). Tracking is accomplished with long open Geiger cells with an octagonal cross section defined by  $100\ \mu\text{m}$  nickel wires. On each side of the source foil there are 10 planes of 32 cells which alternate between vertical and horizontal orientations. Collectively the cells provide

Table 2. Summary of the best results on the  $2\beta\lambda^0$ -decay with  $n = 1$ . All limits are presented at the 90% CL. The dispersion of  $\langle g_{ee} \rangle$  values is due to uncertainties in the NME calculation. The NME from the following works were used:  $^{48}\text{Ca}$  - [29, 30, 31],  $^{150}\text{Nd}$  - [32, 33, 34, 35], and others - [16, 24, 31, 33, 34, 35, 36, 37].

Nucleus	$T_{1/2}, y$	$\langle g_{ee} \rangle$
$^{48}\text{Ca}$	$> 7.2 \cdot 10^{20}$ [25]	$< (5.3 - 8.8) \cdot 10^{-4}$
$^{76}\text{Ge}$	$> 7.9 \cdot 10^{21}$ [26]	$< (2.6 - 7.5) \cdot 10^{-4}$
$^{82}\text{Se}$	$> 2.4 \cdot 10^{21}$ [23]	$< (2.3 - 4.3) \cdot 10^{-4}$
$^{96}\text{Zr}$	$> 3.9 \cdot 10^{20}$ [24]	$< (2.6 - 4.9) \cdot 10^{-4}$
$^{100}\text{Mo}$	$> 3.1 \cdot 10^{21}$ [17]	$< (1 - 4.3) \cdot 10^{-4}$
$^{116}\text{Cd}$	$> 1.2 \cdot 10^{21}$ [16]	$< (1.2 - 4.4) \cdot 10^{-4}$
$^{128}\text{Te}$	$> 2 \cdot 10^{24}$ (geochemical)[15]	$< (0.7 - 1.4) \cdot 10^{-4}$
$^{130}\text{Te}$	$> 0.8 \cdot 10^{21}$ (geochemical)[15]	$< (2.8 - 6.8) \cdot 10^{-4}$
$^{136}\text{Xe}$	$> 7.2 \cdot 10^{21}$ [27]	$< (1.3 - 3.8) \cdot 10^{-4}$
$^{150}\text{Ne}$	$> 2.8 \cdot 10^{20}$ [28]	$< (1 - 5.4) \cdot 10^{-4}$

three-dimensional tracking of charged particles.

A calorimeter made of scintillators covers two vertical opposing sides of the tracking volume. It consisted of two planes of 64 scintillators for the  $^{100}\text{Mo}$  measurements and 25 scintillators for the  $^{116}\text{Cd}$ ,  $^{82}\text{Se}$  and  $^{96}\text{Zr}$  measurements (12 cm $\times$ 12 cm $\times$ 2.25 cm and 19 cm $\times$ 19 cm $\times$ 10 cm, respectively). In the last case low radioactivity photomultiplier tubes (PMT) were used. Finally, the tracking volume and scintillators were surrounded by a lead (5 cm) and iron (20 cm) shield.

## 2.1. Performance

Details of the performances and parameters of NEMO-2 are described elsewhere [16, 21, 22, 23, 24] while the most salient characteristics are briefly outlined here. As mentioned above, the three-dimensional measurements of charged particle tracks are provided by the array of Geiger cells. The transverse position is given by the drift time and the longitudinal position by the plasma propagation times. The transverse resolution is 500  $\mu\text{m}$  and the longitudinal resolution is 4.7 mm. Track reconstruction is accomplished with the tracking method based on the Kalman filter [38]. The calorimeter energy resolution (FWHM) is 18% at 1 MeV with a time resolution of 275 ps (550 ps at

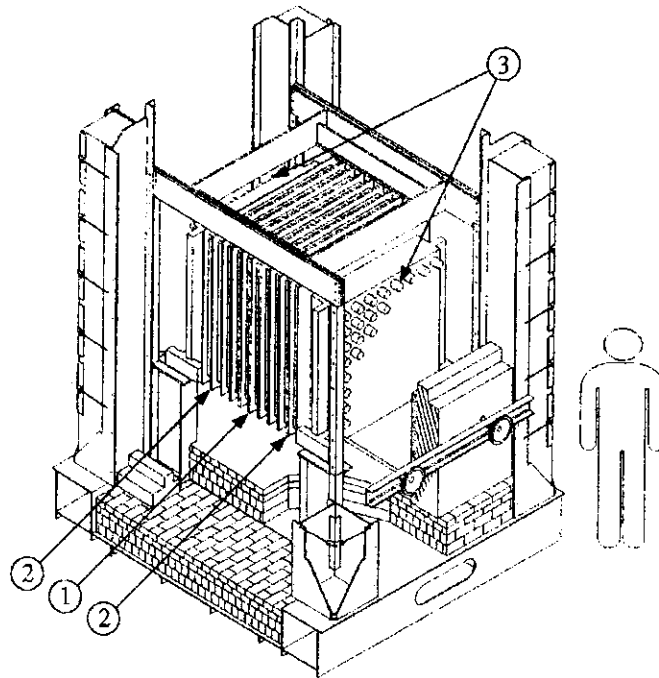


Figure 2. The NEMO-2 detector without shielding: (1) central frame with the source plane capable of supporting plural source foils, (2) ten frames of  $2 \times 32$  Geiger cells for tracking, (3) scintillator array.

0.2 MeV). A laser and fiber optics device is used to check the stability of the scintillation detectors.

## 2.2 Event definition

An electron is defined by a track linking the source foil and one scintillator. The maximum scattering angle along the track has to be less than  $20^\circ$  to reject hard scattering situations. A photon is recognized as one or two adjacent fired scintillators without an associated particle track. For photons and electrons an energy deposited greater than 200 keV is required in order to obtain sufficiently good time resolution. The two-electron events are defined by two tracks which have a common vertex and are associated with two fired scintillators with a deposited energy of at least 200 keV in each one. In the analysis a two-electron event is identified as  $(2e)$ , electron-photon event as  $(e\gamma)$ . A more detailed description of the analysis procedure can be found in references [16, 22, 23, 24].

### 2.3 Source-foils parameters

Natural (163g) and  $^{100}\text{Mo}$  enriched (172g) molybdenum metallic foils were manufactured using a standard rolling technology. They were studied in the first experiment. The enriched and natural foils each defined half of the central plane. The second experiment used natural (143g) and  $^{116}\text{Cd}$  enriched (152g) cadmium metallic foils. The third experiment involved selenium and zirconium sources, which were composed of strips that were produced using a special technique to deposit the material with a binder on mylar films. Masses of enriched materials were  $m_{\text{Se}} = 157\text{g}$  and  $m_{\text{Zr}} = 20.5\text{g}$  and natural were  $m_{\text{Se}} = 134\text{g}$  and  $m_{\text{Zr}} = 18.3\text{g}$ . The Se was placed in the outer region of the central plane and Zr foils in the inner portion of the central plane. The thicknesses of the foils were approximately 40-50 mg/cm<sup>2</sup> for all foils.

Values of the different contaminations in the foils were obtained with the NEMO - 2 detector by analysing electron-gamma and single-electron events, as explained in the sections devoted to backgrounds. These results were compared with HPGe detector measurements.

## 3. Backgrounds

Backgrounds for the NEMO-2 detector had "internal" and "external" origins. Events connected with natural samples were used to estimate the external background in the enriched samples.

The "external" background is due to photons coming from outside of the tracking detector and interacting with the source foils or with the scintillators. Compton electrons produced in the scintillators and crossing the tracking device were rejected by time-of-flight analysis. Compton electrons produced in the source foils can generate a secondary electron by Möller scattering. A double Compton effect or pair production is seen as a 2e event (NEMO-2 could not distinguish between  $e^+$  and  $e^-$ ). These 2e background events cannot be rejected by time-of-flight cuts. The dominant contribution to the external background comes from the flux of photons emitted by radon located between the tracking detector and the shielding. Another source of background is due to the flux of photons emitted by the PMTs.

Radioactive pollution in the source foils produces a background identified as "internal". An electron which gives rise to the Möller effect, or is associated with an internal conversion electron, or a Compton electron can produce a 2e background event.



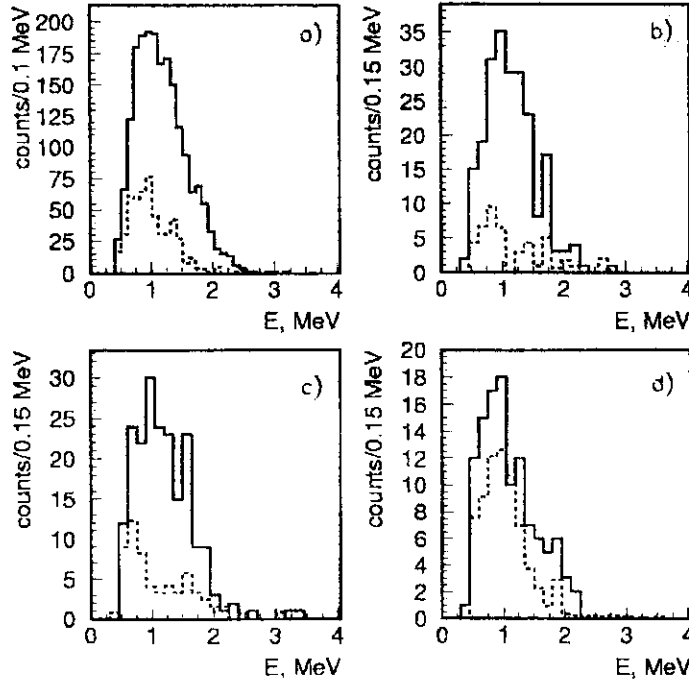


Figure 3. The 2e events (solid line) and estimated backgrounds (dashed line) for (a)  $^{100}\text{Mo}$ , (b)  $^{116}\text{Cd}$ , (c)  $^{82}\text{Se}$  and (d)  $^{96}\text{Zr}$ .

Most of the 2e background events are due to double Compton or knocked Möller electrons with small angles between the two electrons. This is not the case for  $2\beta 2\nu$  decay, where the angles are wide. To improve the signal-to-background ratio the cut  $\cos(\theta_{12}) < 0.6$  on the angle between two electrons, ( $\theta_{12}$ ), was applied in the 2e event selection for the measurements with  $^{116}\text{Cd}$ ,  $^{82}\text{Se}$  and  $^{96}\text{Zr}$ . In the experiment with  $^{100}\text{Mo}$  there were large statistics and this cut was not required.

## 4. Experimental Results

### 4.1 Analysis methods of Experimental Data

The experimental data from enriched samples are shown in Fig. 3 as solid line histograms. The sums of external and internal backgrounds for the different experiments are presented as dashed line histograms. The detection efficiencies for the decays depend on the energy of the electrons and were calculated for all four nuclei, for all the Majoron modes (spectral indices  $n = 1, 3$  and  $7$ ) and for the double beta-decay ( $n = 5$ ) by a Monte-Carlo simulations with the GEANT 3.21 code.

Obtaining limits on the different modes was performed by two methods. In

Table 3. Limits on  $T_{1/2}(y)$  at 90% CL for decays with Majoron emission, estimated via the Helene formula.

Nucleus	$^{100}\text{Mo}$	$^{116}\text{Cd}$	$^{82}\text{Se}$	$^{96}\text{Zr}$
$n = 1$	$> 5.0 \cdot 10^{20}$ [22]	$> 1.2 \cdot 10^{21}$ [16]	$> 2.4 \cdot 10^{21}$ [23]	$> 3.5 \cdot 10^{20}$ [24]
$n = 3$	$> 9.9 \cdot 10^{19}$	$> 4.6 \cdot 10^{20}$	$> 1.1 \cdot 10^{21}$	$> 6.3 \cdot 10^{19}$
$n = 7$	$> 1.7 \cdot 10^{20}$	$> 2.0 \cdot 10^{20}$	$> 3.7 \cdot 10^{20}$	$> 5.1 \cdot 10^{19}$

Table 4. Limits on  $T_{1/2}$  at 90% CL for decays with Majoron emission, estimated with help of likelihood function.

Nucleus	$^{100}\text{Mo}$	$^{116}\text{Cd}$	$^{82}\text{Se}$	$^{96}\text{Zr}$
$n = 1$	$> 6.0 \cdot 10^{20}$	$> 9.2 \cdot 10^{20}$	$> 2.3 \cdot 10^{21}$	$> 3.1 \cdot 10^{20}$
$n = 3$	$> 1.6 \cdot 10^{20}$	$> 3.5 \cdot 10^{20}$	$> 6.3 \cdot 10^{20}$	$> 6.3 \cdot 10^{19}$
$n = 7$	$> 4.1 \cdot 10^{19}$	$> 4.1 \cdot 10^{19}$	$> 1.1 \cdot 10^{20}$	$> 2.4 \cdot 10^{19}$

the first one we estimated  $T_{1/2}^{2\beta 2\nu}$  from our measurements. Then one can get limits on the Majoron mode if the  $2\beta 2\nu$  and background are known and used as expected averages in the Helene formula [39] for Poisson processes:

$$\text{CL}(N) = 1 - e^{-(\mu_b + N)} \sum_{n=0}^{n_0} \frac{(\mu_b + N)^n}{n!} / e^{-\mu_b} \sum_{n=0}^{n_0} \frac{\mu_b^n}{n!}, \quad (3)$$

where  $\mu_b$  is the expected average number of events in an interval and is defined by the sum of  $2\beta 2\nu$  and background events,  $n_0$  is the number of observed events in the same interval, and  $N$  is the limit on the mean number of events from a signal. The dependant variable in this equation is the parameter  $N$  while the  $\text{CL}(N)$  is fixed at 90%.

If one considers the existence of both  $2\beta 2\nu$  and Majoron decay modes, then the  $T_{1/2}^{2\beta 2\nu}$  estimation in some models should not depend on the existence or absence of decays with the emission of  $\chi^0$ . This is applicable for  $2\beta\chi^0$  with spectral index  $n = 1$ , where the  $2\beta 2\nu$  and Majoron spectra profiles peak in different energy regions (Fig. 1). This was done in previous works [16, 22, 23, 24]. Results for all nuclei are given in Table 3. Also shown, for comparison only, are the calculations by the Helene formula method for modes with other spectral indices.

In the case when shapes of the spectra are similar one cannot use the Helene formula, and should follow another method. If one considers the Majoron modes as existing decay channels similar to  $2\beta 2\nu$ , then the experiment is the

sum of two processes,  $2\beta 2\nu$  decay and decay with  $\chi^0$  emission. Thus, one cannot know the expected number of  $2\beta 2\nu$  decays and should set a limit on the decays with Majoron emission by analysing the deviation in the shape of the experimental data calculated for  $2\beta 2\nu$  decay. This can be done with the likelihood function.

Here the experimental spectrum was again treated as a histogram. One then needs to take into account that the distribution of the events in each bin is a Poisson one and independent of the others. Thus, one constructs the likelihood function as:

$$L(N_\beta, N_\chi) = \prod_{i=n_1}^{n_2} \frac{e^{-(N_\beta \eta_{\beta i} + N_\chi \eta_{\chi i} + N_{\text{bgr } i})}}{N_{\text{exp } i}!} (N_\beta \eta_{\beta i} + N_\chi \eta_{\chi i} + N_{\text{bgr } i})^{N_{\text{exp } i}} \quad (4)$$

where  $n_1$  and  $n_2$  are the bin numbers of the energy interval,  $N_{\text{exp } i}$  is the number of experimental events in the  $i$ -th bin,  $N_{\text{bgr } i}$  is the expected number of background events, and  $\eta_{\beta i}$  and  $\eta_{\chi i}$  are the Monte-Carlo simulated efficiencies of  $2\beta 2\nu$  and Majoron decays in the  $i$ -th bin. Finally,  $N_\beta$  and  $N_\chi$  are the average numbers of decays and they are considered as free parameters.

To find the confidence level for the upper limit on the mean number of decays with Majoron emission ( $N_{\chi \text{up}}$ ) this function (4) has to be normalized and then integrated over all possible values of  $N_\beta$  and  $N_\chi$  from 0 to  $N_{\chi \text{up}}$ :

$$\text{CL}(N_{\chi \text{up}}) = \frac{\int_0^{N_{\chi \text{up}}} dN_\chi \int_0^\infty dN_\beta L(N_\beta, N_\chi)}{\int_0^\infty dN_\chi \int_0^\infty dN_\beta L(N_\beta, N_\chi)} \quad (5)$$

Again, this is an equation for the free parameter  $N_{\chi \text{up}}$ , where  $\text{CL}(N_{\chi \text{up}})$  is fixed. To simplify the calculation in the case of  $^{100}\text{Mo}$ , for bins with a large number of the events ( $> 14$  events) the Poisson distribution was replaced by a Gaussian distribution. The results are presented in Table 4.

## 4.2 Results and Discussion.

The half-life limits for different isotopes and decay modes are presented in Tables 3 and 4. Using the half-lives one can get limits on the coupling constants for different Majoron models via the relations (6) and (7).

$$T_{1/2}^{-1} = | \langle g_{ee} \rangle |^2 |M|^2 G \text{ for } 2\beta\chi^0, \quad (6)$$

Table 5. The pn-QRPA nuclear matrix elements for different nuclei. For  $^{82}\text{Se}$ ,  $^{100}\text{Mo}$  and  $^{116}\text{Cd}$  NME are taken from [18]. For  $^{96}\text{Zr}$  the  $M_F - M_{GT}$  is presented in [24], the  $M_{CR}$  value is the lowest among the other nuclei which is taken as a conservative estimation, and for the  $M_{F\omega^2} - M_{GT\omega^2}$  used the same estimate as for the other nuclei in [18].

Nucleus	$M_F - M_{GT}$	$M_{CR}$	$M_{F\omega^2} - M_{GT\omega^2}$
$^{82}\text{Se}$	4.03	0.14	$10^{-3}$
$^{100}\text{Mo}$	4.86	0.16	$10^{-3}$
$^{116}\text{Cd}$	3.29	0.10	$10^{-3}$
$^{96}\text{Zr}$	5.58	0.10	$10^{-3}$

Table 6. Phase-space integrals ( $G$  [ $\text{y}^{-1}$ ]) for different nuclei and models of decay [18]. Zr phase space for  $n=1$  is taken from [40], and for  $n = 3$  and 7 it is calculated following the formulas of [14].

Nucleus	$2\beta\chi^0, n = 1$	$2\beta\chi^0, n = 3$	$2\beta\chi^0\chi^0, n = 3$	$2\beta\chi^0\chi^0, n = 7$
$^{82}\text{Se}$	$1.03 \cdot 10^{-15}$	$3.49 \cdot 10^{-18}$	$1.01 \cdot 10^{-17}$	$7.73 \cdot 10^{-17}$
$^{100}\text{Mo}$	$1.80 \cdot 10^{-15}$	$7.28 \cdot 10^{-18}$	$1.85 \cdot 10^{-17}$	$1.54 \cdot 10^{-16}$
$^{116}\text{Cd}$	$1.75 \cdot 10^{-15}$	$6.95 \cdot 10^{-18}$	$1.60 \cdot 10^{-17}$	$1.03 \cdot 10^{-16}$
$^{96}\text{Zr}$	$1.24 \cdot 10^{-15}$	$1.07 \cdot 10^{-17}$	$2.81 \cdot 10^{-17}$	$3.26 \cdot 10^{-16}$

$$T_{1/2}^{-1} = | \langle g_{ee} \rangle |^4 |M|^2 G \text{ for } 2\beta\chi^0\chi^0, \quad (7)$$

The relevant matrix elements  $M$  and values of phase spaces  $G$  are presented in Tables 5 and 6. Using the data from Table 4 the limits on the coupling constants are calculated and presented in Table 7. In addition, the limits on Majoron-neutrino coupling constants obtained in the  $^{76}\text{Ge}$  experiment [18] are presented. Note that for  $^{100}\text{Mo}$  and  $^{116}\text{Cd}$  there were also limits obtained on decays with two Majoron emission ( $n = 3$ ) for which the limits are  $> 5.3 \times 10^{19}$  years (68% CL) [19] and  $> 2.6 \times 10^{20}$  years (90% CL) [20], respectively.

To summarize the results reported here more thoroughly one can note the following. For  $^{100}\text{Mo}$  the limit on decays with  $n = 3$  obtained here is three times higher than that in [19], while the limit on decays with  $n = 7$  is given for the first time. The result for  $n = 1$  [22] is several times lower than in [17].

The limit on  $^{116}\text{Cd}$  decays with  $n = 3$  is two times higher than that in [20]. The limit on decays with  $n = 7$  is presented for the first time. The limit on decays with Majoron emission for  $n = 1$ , obtained in [20], coincides with the

Table 7. Limits on the Majoron coupling constant  $\langle g_{\ell\ell} \rangle$  at the 90% CL for  $^{82}\text{Se}$ ,  $^{96}\text{Zr}$ ,  $^{100}\text{Mo}$  and  $^{116}\text{Cd}$ .  $^{76}\text{Ge}$  results are presented for comparison.

model	mode	n	$^{82}\text{Se}$	$^{96}\text{Zr}$	$^{100}\text{Mo}$	$^{116}\text{Cd}$	$^{76}\text{Ge}$ [18]
IB	$2\beta\lambda^0$	1	$< 1.6 \cdot 10^{-4}$	$< 2.6 \cdot 10^{-4}$	$< 2.0 \cdot 10^{-4}$	$< 2.1 \cdot 10^{-4}$	$< 2.3 \cdot 10^{-4}$
IC	$2\beta\lambda^0$	1	$< 1.6 \cdot 10^{-4}$	$< 2.6 \cdot 10^{-4}$	$< 2.0 \cdot 10^{-4}$	$< 2.1 \cdot 10^{-4}$	$< 2.3 \cdot 10^{-4}$
ID	$2\beta\lambda^0\lambda^0$	3	$< 3.5$	$< 4.7$	$< 4.3$	$< 3.6$	$< 4.1$
IE	$2\beta\lambda^0\lambda^0$	3	$< 3.5$	$< 4.7$	$< 4.3$	$< 3.6$	$< 4.1$
IIB	$2\beta\lambda^0$	1	$< 1.6 \cdot 10^{-4}$	$< 2.6 \cdot 10^{-4}$	$< 2.0 \cdot 10^{-4}$	$< 2.1 \cdot 10^{-4}$	$< 2.3 \cdot 10^{-4}$
IIC	$2\beta\lambda^0$	3	$< 0.15$	$< 0.36$	$< 0.19$	$< 0.20$	$< 0.18$
IID	$2\beta\lambda^0\lambda^0$	3	$< 3.5$	$< 4.7$	$< 4.3$	$< 3.6$	$< 4.1$
IIE	$2\beta\lambda^0\lambda^0$	7	$< 3.3$	$< 3.2$	$< 3.6$	$< 3.9$	$< 3.3$
IIF	$2\beta\lambda^0$	3	$< 0.15$	$< 0.36$	$< 0.19$	$< 0.20$	$< 0.18$

results of our earlier work [16].

Next, for  $^{96}\text{Zr}$  all the limits are presented for the first time in a direct counting experiment. They can be compared with the geochemical experiments, which give a half-life,  $T_{1/2} = (3.9 \pm 0.9) \cdot 10^{19}$  years. This result is treated as a half-life for  $2\beta 2\nu$ , while  $T_{1/2} > 3 \cdot 10^{19}$  y should be treated as a limit on all possible transitions  $^{96}\text{Zr} \rightarrow ^{96}\text{Mo}$ , such as those involving Majoron emission processes. The NEMO-2 limits exceed those obtained from geochemical experiments for all types of decays with Majoron emission ( $n = 1, 3$  and  $7$ ).

Finally, the  $^{82}\text{Se}$  results for  $n = 3$  and  $7$  are presented here for the first time. Note that the result for the transition with  $n = 1$  [23] is also the best for  $^{82}\text{Se}$ . Analysis of the results documented above, show that the best limits on the coupling constant for all "non-standard" decays with Majoron emission ( $n = 3$  and  $7$ ) were obtained with the NEMO-2 experiment with  $^{82}\text{Se}$ .

## 5. Conclusion

Though NEMO-2 was developed as a prototype for NEMO-3 [41], the limits on  $2\beta$ -decay processes with Majoron emission are among the best. In particular limits on "non-standard" Majoron with  $n = 3$  and  $7$  are more stringent than the limits coming from other experiments. The current plan is to start measurements with the NEMO-3 detector at the end of the year 2000. The total mass of the  $2\beta$ -sources will be increased to 10-15 kg, and different isotopes ( $^{100}\text{Mo}$ ,  $^{82}\text{Se}$ ,  $^{116}\text{Cd}$ ,  $^{130}\text{Te}$ ,  $^{150}\text{Nd}$  and  $^{96}\text{Zr}$ ) will be investigated. The sensitivity to half-life measurements for processes with Majoron emission ( $n = 1, 3$  and  $7$ ) will be improved by 10 to 100 times, while the limits on the

coupling constant will be improved by 3 to 10 times, depending on the type of decay.

## Acknowledgement

The authors would like to thank the Fréjus Underground Laboratory staff for their technical assistance in running the experiment, and are very thankful to V.I. Tretyak for coding new Majoron decay modes. Portions of this work were supported by the Russian Foundation for Branch Investigations (RFBI) under contract 97-02-17344, by INTAS under grant 96-0589 and by US, Department of Energy Grant DE-FG02-90ER40553.

---

## References

- [1] Chikashige Y., Mohapatra R.N., Peccei R.D. // *Phys. Rev. Lett.* 1980 Vol.45, P.1926 / *Phys. Lett. B.* 1981 Vol.98, P.265.
- [2] Aulakh C., Mohapatra R. // *Phys. Lett. B.* 1982 Vol.119, P.136.
- [3] Gelmini G., Roncadelli M. // *Phys. Lett. B.* 1981 Vol.99, P.1411.
- [4] Georgi H.M., Glashow S.L., Nussinov S. // *Nucl. Phys. B.* 1981 Vol.193, P.297.
- [5] Barger V. et al. // *Phys. Rev. D.* 1982 Vol.26, P.218.
- [6] Deshpande N.G. // *Proc. Conf. on Neutrino Masses and Neutrino Astrophysics.* Edited by Barger V. et al. Singapore: World Scientific, 1987 P.78.
- [7] Caso C. et al. (Particle Data Group)// *European Physical Journal C.* 1998 Vol.3, P.1.
- [8] Berezhiani Z.G., Smirnov A. Yu., Valle J.W.F. // *Phys. Lett. B.* 1992 Vol.291,P.99.
- [9] Mohapatra R.N., Pal P.B.. *Massive Neutrinos in Physics and Astrophysics.* Singapore: World Scientific, 1991.
- [10] Mohapatra R.N., Takasugi E. // *Phys. Lett. B.* 1988 Vol.211, P.192.
- [11] Burgess C.P., Cline J.M. // *Phys. Lett.* 1993 Vol.B298, P.141 / *Phys. Rev. D.* 1994 Vol.49, P.5925.

- [12] Bamert P., Burgess C.P., Mohapatra R.N. // Nucl. Phys. B. 1995 Vol.449, P.25.
- [13] Carone C.D. // Phys. Lett. B. 1993 Vol.308, P.85.
- [14] Hirsch M. et al. // Phys. Lett. B. 1996 Vol.372, P.8.
- [15] Manuel O.K. // J. Phys. G. 1991 Vol.17, P.221.
- [16] Arnold R. et al. // Z. Phys. C. 1996 Vol.72, P.239.
- [17] Ejiri H. et al. // Nucl. Phys. A. 1996 Vol.611, P.85.
- [18] Gunther M. et al. // Phys. Rev. D. 1996 Vol.54, P.3641.
- [19] Tanaka J., Ejiri H. // Phys.Rev. D. 1993 Vol.48, P.5412.
- [20] Danevich F.A. et al. // Nucl. Phys. A. 1998 Vol.643, P.317.
- [21] Arnold R. et al. // Nucl. Instr. Meth. A. 1995 Vol.354, P.338.
- [22] Dassie D. et al. // Phys. Rev. D. 1995 Vol.51, P.2090.
- [23] Arnold R. et al. // Nucl. Phys. A. 1998 Vol.636, P.209.
- [24] Arnold R. et al. // Nucl. Phys. A. 1999, Vol.658, P.299.
- [25] Barabash A.S. // Phys. Lett. B. 1989 Vol.216, P.257.
- [26] Gunther M. et al. // Phys. Rev. D. 1997 Vol.55, P.54.
- [27] Luescher R. et al. // Phys. Lett. B. 1998 Vol.434, P.407.
- [28] De Silva A., Moe M.K., Nelson M.A., Vient M.A. // Phys. Rev. C. 1997 Vol.56, P.2451
- [29] Haxton W.C. and Stephenson G.S. // Prog. Part. Nucl. Phys. 1984 Vol.12, P.409.
- [30] Retamosa J., Caurier E. and Nowacki F. // Phys. Rev. C. 1995 Vol.51, P.371.
- [31] Caurier E. et al. // Nucl. Phys. A. 1999 Vol.654, P.973c.
- [32] Hirsch J.G., Castanos O. and Hess P.O. // Nucl. Phys. A. 1995 Vol.582, P.124.
- [33] Muto K., Bender E. and Klapdor H.V. // Z. Phys. A. 1989 Vol.334, P.187.

- [34] Tomoda T. // Rep. Prog. Phys. 1991 Vol.54, P.53.
- [35] Simkovic F. et al. // Phys. Rev. C. 1999 Vol.60, P.055502.
- [36] Engel J., Vogel P. and Zirnbauer M.R. // Phys. Rev. C. 1988 Vol.37, P.73.
- [37] Caurier E. et al. // Phys. Rev. Lett. 1996 Vol.77, P.1954.
- [38] Billoir P. // Nucl. Instr. Meth. A. 1984 Vol.255, P.352
- [39] Helene O. // Nucl. Instr. Meth. B. 1983 Vol.212, P.319 / Particle Data Group Phys. Rev. D. 1994 Vol.50, P.1281
- [40] Suhonen J., Civitarese O. // Phys. Rep. 1998 Vol.300, P.123
- [41] NEMO-3 Proposal // LAL preprint 1994 Number 94-29.